Design of a novel cutter for manufacturing helical cutting tools

S-L Chang* and **H-C Tseng**
Department of Power Mechanical Engineering, National Formosa University, Huwei, Yunlin, Taiwan

The manuscript was received on 12 December 2003 and was accepted after revision for publication on 23 November 2004.

DOI: 10.1243/095440605X16901

Abstract: Owing to the complex geometry of helical cutting tools, several manufacturing processes are required to produce the profile of the cutter and the cutting angles. If the traditional method of manufacture were used, the cost would be frustratingly expensive. In this paper, a novel straight-sided hob cutter design consisting of two curved cutting edges and three straight cutting edges with different pressure angles is proposed. By applying designed rake profile equations of a hob cutter, the principle of coordinate transformation, the theory of differential geometry, and the theory of gearing, a mathematical model of the helical cutting tool is derived. In addition, the cutting angles, the condition of full undercutting, and the width of the top land of the cutter are also studied. The novelty of the design is such that the multiangles of the helical cutting tool can be manufactured in one hobbing process, thereby simplifying the manufacturing process. The results and concepts proposed in the paper will be beneficial as design guidance for tool designers, will enhance the manufacturing processes of helical cutting tools, and will assist tool-related industries in upgrading their technology and competitiveness.

Keywords: undercut, cutter, helical cutting tool

1 INTRODUCTION

Helical cutting tools are very important as they are frequently used in the manufacture of machine parts. The traditional manufacturing process of these cutting tools involves sophisticated techniques such as milling and several grinding processes to generate the multicutting angles, namely, the radial rake angle, the relief angle, and the clearance angle. This often results in expensive manufacturing cost.

Undercutting is a phenomenon that causes weakness at the root of the manufactured gears. Engineers have been using shifted gears, modified tooth profiles, or changing pressure angles to overcome undercutting in gears. In this paper, however, this undesirable phenomenon is applied to manufacture a helical cutting tool using a novel straight-sided hob with three different pressure angles. Undercutting is applied to generate the radial rake angle with the smallest pressure angle, while the two largest pressure angles generate the relief angle, the clearance angle, and the chip flute. All these are carried out simultaneously in a single hobbing process, which significantly reduces the cost of production.

Hobbing of gears is the most frequent and effective manufacturing process used in the gear industry. New methods in improving the precision of hobbing were introduced by researchers [**1**–**5**]. The most popular method to simulate the generating process of a hob cutter was done by the rack cutter [**6**, **7**]. Recent research relevant to the hobbing process of a hob cutter includes work by Chang *et al.* [**8**, **9**], who studied the manufacturing of modified helical and elliptical gears. Chang [**10**] simulated the hobbing process through a computer numerically controlled (CNC) hobbing machine. More recently, Kapelevich [**11**] investigated the hobbing of an unsymmetrical involute tooth profile. However, these published works offered little systematic and in-depth discussion on the design and generation of the cutting tool tooth profile. In particular, there

**Corresponding author: Department of Power Mechanical Engineering, National Formosa University, 64 Wun Hua Road, Huwei, 632 Yunlin, Taiwan.*

was no discussion of the design, analysis, and mathematical model of a hob cutter capable of generating a helical cutter with multiangles.

Liu and Chang [**12**] proposed a rack cutter with three different pressure angles and a full radius corner to generate a helical cutter. This multiangle cutting tool cutter is the research topic in this paper, where a full study on the undercutting phenomenon, the width of the top land, and the cutting angles is carried out. This research is beneficial as design guidance for tool designers, and it also enhances machining efficiencies and competitiveness in the tool industry.

2 NEW DESIGN OF THE RACK CUTTER PROFILE

Hob cutters with a straight-sided cutting face are commonly used in the manufacture of involute gears. Improper parameter design of the gears will cause undercutting at the root of the gears. However, with proper selection of the hob cutter parameters, a straight-sided hob cutter using the phenomenon of undercutting can be used to generate the cutting tool profile of a helical cutting tool, an example of which is shown in Fig. 1. The cutting face of the hob cutter can be divided into six regions, i.e. the left cutting face (I), the right cutting face (II), the fillet cutting faces (III and IV), the top land cutting face (V), and the chamfering cutting face (VI). The profile of the cutter is similar to that of an ordinary hob cutter except for the three pressure angles, i.e. the two largest pressure angles in regions I and VI and the smallest pressure angle in region II, which uses undercutting to generate the tool shape and forms the radial rake angle. Region I, which has the larger pressure angle, generates the involute shape of the main body of the helical cutting tool. Region VI, with the largest pressure angle, generates the chamfering of the cutting tool, thus forming the clearance and relief angles of the helical cutting tool. By applying the equations of the designed rake profiles of the hob cutters, the principle of coordinate transformation, the theory of differential geometry, and the theory of gearing, a mathematical model of the helical cutting tool can be derived.

Here, O_a is defined as the origin of the coordinate system $S_a(X_a, Y_a, Z_a)$ located at the middle of the rack cutter body, ψ_L is the pressure angle of the left cutting face, ψ_R is the pressure angle of the right cutting face, ψ_3 is the pressure angle of the chamfering cutting face, HKW is the addendum of the rack cutter (dedendum of the helical cutting tool), HFW is the dedendum of the rack cutter (addendum of the helical cutting tool), R is the radius of the rack cutter fillet, and $2b_0$ is the tooth thickness of the rack cutter (tooth spacing of the helical cutting tool).

2.1 Equations of the rack cutter

The equations of the six regions of the rack cutter can be shown in the $S_a(X_a, Y_a, Z_a)$ coordinate system and presented as follows.

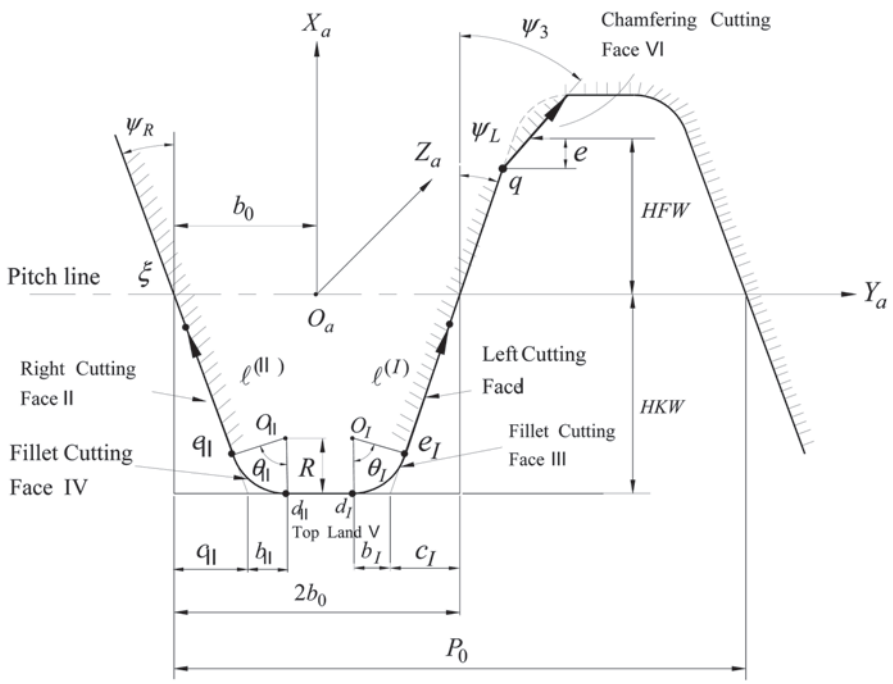

Fig. 1 Normal section tooth profile of the hob cutter

2.1.1 Left cutting face (region I)

The coordinates of the origin of region I, e_{I}, in Fig. 1 are

$$x_{\mathrm{a}}^{(e_{\mathrm{I}})} = R - \mathrm{HKW} - R\sin\psi_{\mathrm{L}} \tag{1}$$

$$y_{\mathrm{a}}^{(e_{\mathrm{I}})} = b_0 - \frac{R}{\tan(45+\psi_{\mathrm{L}}/2)} - \mathrm{HKW}\tan\psi_{\mathrm{L}} + R\cos\psi_{\mathrm{L}} \tag{2}$$

where parameter $\ell^{(\mathrm{I})}$ indicates the position on region I.

The equation of the left cutting face can thus be presented in the S_{a} coordinate system as follows

$$\boldsymbol{r}_{\mathrm{a}}^{(\mathrm{I})} = \begin{bmatrix} R - \mathrm{HKW} - R\sin\psi_{\mathrm{L}} + \ell^{(\mathrm{I})}\cos\psi_{\mathrm{L}} \\ b_0 - \dfrac{R}{\tan(45+\psi_{\mathrm{L}}/2)} - \mathrm{HKW}\tan\psi_{\mathrm{L}} \\ \quad + R\cos\psi_{\mathrm{L}} + \ell^{(\mathrm{I})}\sin\psi_{\mathrm{L}} \\ 0 \\ 1 \end{bmatrix} \tag{3}$$

2.1.2 Right cutting face (region II)

The coordinates of the origin of region II, e_{II}, in Fig. 1 are

$$x_{\mathrm{a}}^{(e_{\mathrm{II}})} = R - \mathrm{HKW} - R\sin\psi_{\mathrm{R}} \tag{4}$$

$$y_{\mathrm{a}}^{(e_{\mathrm{II}})} = -b_0 + \frac{R}{\tan(45+\psi_{\mathrm{R}}/2)} + \mathrm{HKW}\tan\psi_{\mathrm{R}} - R\cos\psi_{\mathrm{R}} \tag{5}$$

where parameter ℓ^{II} indicates the position on the right cutting face.

The equation of the right cutting face can thus be presented in the S_{a} coordinate system as follows

$$\boldsymbol{r}_{\mathrm{a}}^{(\mathrm{II})} = \begin{bmatrix} R - \mathrm{HKW} - R\sin\psi_{\mathrm{R}} + \ell^{(\mathrm{II})}\cos\psi_{\mathrm{R}} \\ -b_0 + \dfrac{R}{\tan(45+\psi_{\mathrm{R}}/2)} + \mathrm{HKW}\tan\psi_{\mathrm{R}} \\ \quad -R\cos\psi_{\mathrm{R}} - \ell^{(\mathrm{II})}\sin\psi_{\mathrm{R}} \\ 0 \\ 1 \end{bmatrix} \tag{6}$$

2.1.3 Fillet cutting face (region III)

In Fig. 1, parameter R is the fillet radius of the rack cutter. The coordinates of the origin of the fillet cutting face, $\mathrm{O_I}$, are

$$x_{\mathrm{a}}^{(\mathrm{O_I})} = R - \mathrm{HKW} \tag{7}$$

$$y_{\mathrm{a}}^{(\mathrm{O_I})} = b_0 - \frac{R}{\tan(45+\psi_{\mathrm{L}}/2)} - \mathrm{HKW}\tan\psi_{\mathrm{L}} \tag{8}$$

where parameter θ_{I} indicates the position on the fillet cutting face.

The equation of the fillet cutting face can thus be presented in the S_{a} coordinate system as follows

$$\boldsymbol{r}_{\mathrm{a}}^{(\mathrm{III})} = \begin{bmatrix} R - \mathrm{HKW} - R\cos\theta_{\mathrm{I}} \\ b_0 - \dfrac{R}{\tan(45+\psi_{\mathrm{L}}/2)} - \mathrm{HKW}\tan\psi_{\mathrm{L}} + R\sin\theta_{\mathrm{I}} \\ 0 \\ 1 \end{bmatrix} \tag{9}$$

2.1.4 Fillet cutting face (region IV)

The coordinates of the origin of the fillet cutting face, $\mathrm{O_{II}}$, are

$$x_{\mathrm{a}}^{(\mathrm{O_{II}})} = R - \mathrm{HKW} \tag{10}$$

$$y_{\mathrm{a}}^{(\mathrm{O_{II}})} = -b_0 + \frac{R}{\tan(45+\psi_{\mathrm{R}}/2)} + \mathrm{HKW}\tan\psi_{\mathrm{R}} \tag{11}$$

where parameter θ_{II} indicates the position on the fillet cutting face.

The equation of the fillet cutting face can thus be presented in the S_{a} coordinate system as follows

$$\boldsymbol{r}_{\mathrm{a}}^{(\mathrm{IV})} = \begin{bmatrix} R - \mathrm{HKW} - R\cos\theta_{\mathrm{II}} \\ -b_0 + \dfrac{R}{\tan(45+\psi_{\mathrm{R}}/2)} + \mathrm{HKW}\tan\psi_{\mathrm{R}} - R\sin\theta_{\mathrm{II}} \\ 0 \\ 1 \end{bmatrix} \tag{12}$$

2.1.5 Top land cutting face (region V)

The top land cutting face is formed between two points d_{II} and d_{I}. The coordinates of d_{II} and d_{I} of the top land cutting face in the S_{a} coordinate system are represented by the equations

$$x_{\mathrm{a}}^{(d_{\mathrm{II}})} = -\mathrm{HKW} \tag{13}$$

$$y_{\mathrm{a}}^{(d_{\mathrm{II}})} = y_{\mathrm{a}}^{(o_{\mathrm{II}})} = -b_0 + \frac{R}{\tan(45+\psi_{\mathrm{R}}/2)} + \mathrm{HKW}\tan\psi_{\mathrm{R}} \tag{14}$$

$$x_{\mathrm{a}}^{(d_{\mathrm{I}})} = -\mathrm{HKW} \tag{15}$$

$$y_{\mathrm{a}}^{(d_{\mathrm{I}})} = y_{\mathrm{a}}^{(o_{\mathrm{I}})} = b_0 - \frac{R}{\tan(45+\psi_{\mathrm{L}}/2)} - \mathrm{HKW}\tan\psi_{\mathrm{L}} \tag{16}$$

where parameter μ indicates the position on the top land cutting face.

The equation of the top land cutting face from point d_{II} to point d_I can thus be represented in the S_a coordinate system as follows

$$\boldsymbol{r}_a^{(V)} = \begin{bmatrix} -\mathrm{HKW} \\ -b_0 + \dfrac{R}{\tan(45 + \psi_R/2)} + \mathrm{HKW}\tan\psi_R - \mu \\ 0 \\ 1 \end{bmatrix} \tag{17}$$

2.1.6 *Chamfering cutting face (region VI)*

The coordinates of the origin of the chamfering cutter face, q, are

$$x_a^{(q)} = \mathrm{HFW} - e \tag{18}$$

$$y_a^{(q)} = b_0 + (\mathrm{HFW} - e)\tan\psi_L \tag{19}$$

where parameter $\ell^{(VI)}$ indicates the position on the chamfering cutting face.

The equation of the chamfering cutting face can thus be represented in the S_a coordinate system as follows

$$\boldsymbol{r}_a^{(VI)} = \begin{bmatrix} \mathrm{HFW} - e + \ell^{(VI)}\cos\psi_3 \\ b_0 + (\mathrm{HFW} - e)\tan\psi_L + \ell^{(VI)}\sin\psi_3 \\ 0 \\ 1 \end{bmatrix} \tag{20}$$

3 EQUATIONS AND UNIT NORMAL VECTORS OF THE HELICAL RACK CUTTER

Non-standard gears can be manufactured by shifting the cutter to the required positions during machining. In the case of a helical rack cutter, the normal section of the rack cutter is translated along the direction of the lead as shown in Figs 2 and 3. In this sense, the equation of the helical rack cutter can be obtained by transforming the equations of the cutting face from the coordinate system of the rack cutter to that of the helical rack cutter. The transformation matrix $[\mathbf{M}_{wa}]$ expressed by

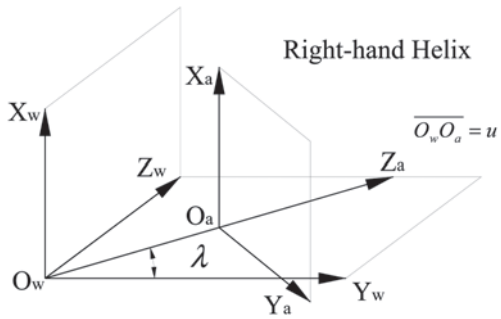

Fig. 2 Coordinate system of the right-hand helix of the rack cutter

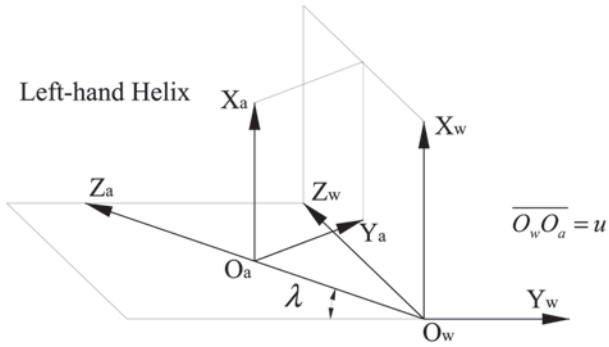

Fig. 3 Coordinate system of the left-hand helix of the rack cutter

$$[\mathbf{M}_{wa}] = \begin{bmatrix} 1 & 0 & 0 & 0 \\ 0 & \sin\lambda & \pm\cos\lambda & \pm u\cos\lambda \\ 0 & \mp\cos\lambda & \sin\lambda & u\sin\lambda \\ 0 & 0 & 0 & 1 \end{bmatrix} \tag{21}$$

indicates the transformation of the rack cutter coordinate system S_a to the helical coordinate system S_w, as shown in Figs 2 and 3. The equation and unit normal vector $\boldsymbol{n}_w$ of the helical rack cutter presented in the S_w coordinate system can thus be obtained. The upper sign of transformation matrix $[\mathbf{M}_{wa}]$ and in the equations of the helical rack cutter (equations (21) to (33)) indicate the right-hand helix of the rack cutter, while the lower sign indicates the left-hand helix. Therefore, the equations of the helical rack cutter in the six regions are as follows.

Left cutting face

$$\boldsymbol{r}_w^{(I)} = [\mathbf{M}_{wa}]\boldsymbol{r}_a^{(I)} \tag{22}$$

$$\boldsymbol{n}_w^{(I)} = \frac{(\partial \boldsymbol{r}_w^{(I)}/\partial\ell^{(I)}) \times (\partial \boldsymbol{r}_w^{(I)}/\partial u)}{\left|(\partial \boldsymbol{r}_w^{(I)}/\partial\ell^{(I)}) \times (\partial \boldsymbol{r}_w^{(I)}/\partial u)\right|}$$

$$= \sin\psi_L \boldsymbol{i}_w - \sin\lambda\cos\psi_L \boldsymbol{j}_w \pm \cos\lambda\cos\psi_L \boldsymbol{k}_w \tag{23}$$

Right cutting face

$$\boldsymbol{r}_w^{(II)} = [\mathbf{M}_{wa}]\boldsymbol{r}_a^{(II)} \tag{24}$$

$$\boldsymbol{n}_w^{(II)} = \frac{(\partial \boldsymbol{r}_w^{(II)}/\partial\ell^{(II)}) \times (\partial \boldsymbol{r}_w^{(II)}/\partial u)}{\left|(\partial \boldsymbol{r}_w^{(II)}/\partial\ell^{(II)}) \times (\partial \boldsymbol{r}_w^{(II)}/\partial u)\right|}$$

$$= -\sin\psi_R \boldsymbol{i}_w - \cos\psi_R \sin\lambda \boldsymbol{j}_w \pm \cos\psi_R \cos\lambda \boldsymbol{k}_w \tag{25}$$

Fillet cutting face (region III)

$$\boldsymbol{r}_{\mathrm{w}}^{(\mathrm{III})} = [\mathbf{M}_{\mathrm{wa}}]\boldsymbol{r}_{\mathrm{a}}^{(\mathrm{III})} \tag{26}$$

$$\begin{aligned}\boldsymbol{n}_{\mathrm{w}}^{(\mathrm{III})} &= \frac{(\partial \boldsymbol{r}_{\mathrm{w}}^{(\mathrm{III})}/\partial\theta_{\mathrm{I}}) \times (\partial \boldsymbol{r}_{\mathrm{w}}^{(\mathrm{III})}/\partial u)}{\left|(\partial \boldsymbol{r}_{\mathrm{w}}^{(\mathrm{III})}/\partial\theta_{\mathrm{I}}) \times (\partial \boldsymbol{r}_{\mathrm{w}}^{(\mathrm{III})}/\partial u)\right|} \\ &= \cos\theta_{\mathrm{I}}\boldsymbol{i}_{\mathrm{w}} - \sin\theta_{\mathrm{I}}\sin\lambda\boldsymbol{j}_{\mathrm{w}} \pm \sin\theta_{\mathrm{I}}\cos\lambda\boldsymbol{k}_{\mathrm{w}}\end{aligned} \tag{27}$$

Fillet cutting face (region IV)

$$\boldsymbol{r}_{\mathrm{w}}^{(\mathrm{IV})} = [\mathbf{M}_{\mathrm{wa}}]\boldsymbol{r}_{\mathrm{a}}^{(\mathrm{IV})} \tag{28}$$

$$\begin{aligned}\boldsymbol{n}_{\mathrm{w}}^{(\mathrm{IV})} &= \frac{(\partial \boldsymbol{r}_{\mathrm{w}}^{(\mathrm{IV})}/\partial\theta_{\mathrm{II}}) \times (\partial \boldsymbol{r}_{\mathrm{w}}^{(\mathrm{IV})}/\partial u)}{\left|(\partial \boldsymbol{r}_{\mathrm{w}}^{(\mathrm{IV})}/\partial\theta_{\mathrm{II}}) \times (\partial \boldsymbol{r}_{\mathrm{w}}^{(\mathrm{IV})}/\partial u)\right|} \\ &= -\cos\theta_{\mathrm{II}}\boldsymbol{i}_{\mathrm{w}} - \sin\theta_{\mathrm{II}}\sin\lambda\boldsymbol{j}_{\mathrm{w}} \\ &\quad \pm \sin\theta_{\mathrm{II}}\cos\lambda\boldsymbol{k}_{\mathrm{w}}\end{aligned} \tag{29}$$

Top land cutting face

$$\boldsymbol{r}_{\mathrm{w}}^{(\mathrm{V})} = [\mathbf{M}_{\mathrm{wa}}]\boldsymbol{r}_{\mathrm{a}}^{(\mathrm{V})} \tag{30}$$

$$\begin{aligned}\boldsymbol{n}_{\mathrm{w}}^{(\mathrm{V})} &= \frac{(\partial \boldsymbol{r}_{\mathrm{w}}^{(\mathrm{V})}/\partial\mu) \times (\partial \boldsymbol{r}_{\mathrm{w}}^{(\mathrm{V})}/\partial u)}{\left|(\partial \boldsymbol{r}_{\mathrm{w}}^{(\mathrm{V})}/\partial\mu) \times \partial \boldsymbol{r}_{\mathrm{w}}^{(\mathrm{V})}/\partial u\right|} \\ &= \boldsymbol{i}_{\mathrm{w}}\end{aligned} \tag{31}$$

Chamfering cutting face

$$\boldsymbol{r}_{\mathrm{w}}^{(\mathrm{VI})} = [\mathbf{M}_{\mathrm{wa}}]\boldsymbol{r}_{\mathrm{a}}^{(\mathrm{VI})} \tag{32}$$

$$\begin{aligned}\boldsymbol{n}_{\mathrm{w}}^{(\mathrm{VI})} &= \frac{\partial \boldsymbol{r}_{\mathrm{w}}^{(\mathrm{VI})}/\partial\ell^{(\mathrm{VI})} \times \partial \boldsymbol{r}_{\mathrm{w}}^{(\mathrm{VI})}/\partial u}{\left|\partial \boldsymbol{r}_{\mathrm{w}}^{(\mathrm{VI})}/\partial\ell^{(\mathrm{VI})} \times \partial \boldsymbol{r}_{\mathrm{w}}^{(\mathrm{VI})}/\partial u\right|} \\ &= \sin\psi_3\boldsymbol{i}_{\mathrm{w}} - \sin\lambda\cos\psi_3\boldsymbol{j}_{\mathrm{w}} \pm \cos\lambda\cos\psi_3\boldsymbol{k}_{\mathrm{w}}\end{aligned} \tag{33}$$

4 LOCUS EQUATION

The locus equations of the helical cutting tool $\boldsymbol{r}_1$ can be obtained by transforming the equations of the cutting face from the coordinate system S_{w} of the helical rack cutter to the S_1 coordinate system of the helical cutting tool.

When a rack cutter is used to cut gears, the relationship between the coordinate systems can be presented as in Fig. 4, where the theoretical pitch surface of the helical rack cutter is tangent to the pitch surface of the helical cutting tool to be cut when the distance shifted, c, is zero. As the theoretical pitch surface of the helical rack cutter, i.e. the Y_{w}–Z_{w} plane, moves towards the helical cutting tool, c is defined as negative. The mathematical model proposed here can then be used to simulate the helical cutting tools with different shifted distances manufactured by the same rack cutter or the hob cutter. In the manufacture of a helical cutting tool, the active pitch surface Y_{d}–Z_{d} translates towards the left while the generated helical cutting tool rotates in the counterclockwise direction. The locus equations of the rack cutter presented in the S_1 coordinate system are shown in equations (35) to (40), where the upper sign indicates the right-hand helix and the lower sign indicates the left-hand helix of the helical cutting tool. The transformation matrix $[\mathbf{M}_{1\mathrm{w}}]$ transforming the S_{w} coordinate system to the S_1 coordinate system is shown as

$$[\mathbf{M}_{1\mathrm{w}}] = [\mathbf{M}_{1\mathrm{h}}\mathbf{M}_{\mathrm{hw}}] = \begin{bmatrix} \cos\phi_1 & -\sin\phi_1 & 0 & r_1\phi_1\sin\phi_1 + (r_1 - c)\cos\phi_1 \\ \sin\phi_1 & \cos\phi_1 & 0 & -r_1\phi_1\cos\phi_1 + (r_1 - c)\sin\phi_1 \\ 0 & 0 & 1 & 0 \\ 0 & 0 & 0 & 1 \end{bmatrix} \tag{34}$$

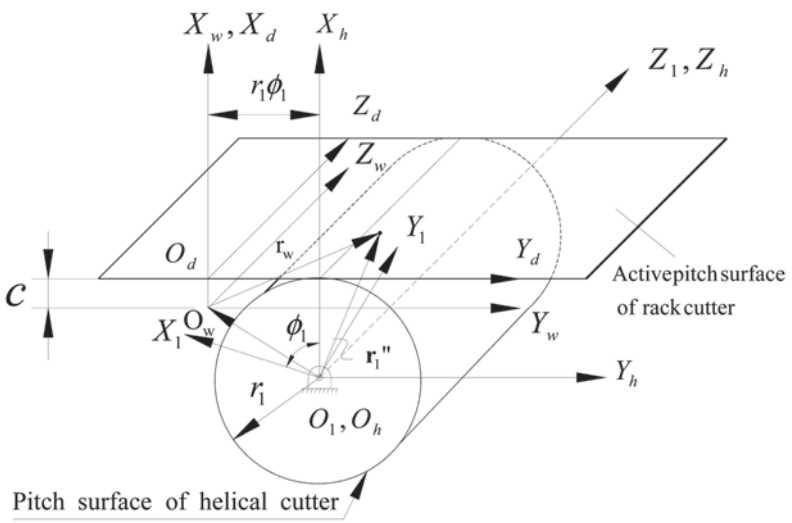

Fig. 4 Coordinate system relationship of the rack cutter and generated gear

Therefore, the locus equations of the rack cutter for the six cutting regions are as follows.

Locus of the left cutting face

$$\boldsymbol{r}_1^{(\mathrm{I})} = [\mathbf{M}_{1\mathrm{w}}]\boldsymbol{r}_{\mathrm{w}}^{(\mathrm{I})} \tag{35}$$

where $\boldsymbol{r}_{\mathrm{w}}^{(\mathrm{I})}$ is shown in equation (22).

Locus of the right cutting face

$$\boldsymbol{r}_1^{(\mathrm{II})} = [\mathbf{M}_{1\mathrm{w}}]\boldsymbol{r}_{\mathrm{w}}^{(\mathrm{II})} \tag{36}$$

where $\boldsymbol{r}_{\mathrm{w}}^{(\mathrm{II})}$ is shown in equation (24).

Locus of the fillet cutting face (region III)

$$\boldsymbol{r}_1^{(\mathrm{III})} = [\mathbf{M}_{1\mathrm{w}}]\boldsymbol{r}_{\mathrm{w}}^{(\mathrm{III})} \tag{37}$$

where $\boldsymbol{r}_{\mathrm{w}}^{(\mathrm{III})}$ is shown in equation (26).

Locus of the fillet cutting face (region IV)

$$\boldsymbol{r}_1^{(\mathrm{IV})} = [\mathbf{M}_{1\mathrm{w}}]\boldsymbol{r}_{\mathrm{w}}^{(\mathrm{IV})} \tag{38}$$

where $\boldsymbol{r}_{\mathrm{w}}^{(\mathrm{IV})}$ is shown in equation (28).

Locus of the top land cutting face

$$\boldsymbol{r}_1^{(\mathrm{V})} = [\mathbf{M}_{1\mathrm{w}}]\boldsymbol{r}_{\mathrm{w}}^{(\mathrm{V})} \tag{39}$$

where $\boldsymbol{r}_{\mathrm{w}}^{(\mathrm{V})}$ is shown in equation (30).

Locus of the chamfering cutting face

$$\boldsymbol{r}_1^{(\mathrm{VI})} = [\mathbf{M}_{1\mathrm{w}}]\boldsymbol{r}_{\mathrm{w}}^{(\mathrm{VI})} \tag{40}$$

where $\boldsymbol{r}_{\mathrm{w}}^{(\mathrm{VI})}$ is shown in equation (32).

5 EQUATION OF MESHING

Figure 4 shows the rack cutter used to generate the helical cutting tool. A relation can be used to obtain the relative velocity of the contact point, $\boldsymbol{V}_{\mathrm{h}}^{(\mathrm{FI})}$. The equation of meshing $\boldsymbol{n} \cdot \boldsymbol{V}_{\mathrm{h}}^{(\mathrm{FI})} = 0$ can then be obtained, which indicates that the unit normal vector is perpendicular to the relative velocity at the contact point by the theory of gearing. From the figure it is clear that the unit normal vector of the cutting face presented in the S_{w} coordinate system is the same as it is in the S_{h} coordinate system, i.e. $\boldsymbol{n}_{\mathrm{w}} = \boldsymbol{n}_{\mathrm{h}}$. The upper sign of equations (46) to (56) indicates the right-hand helix while the lower sign indicates the left-hand helix of the helical cutting tool. The derived equations are shown as follows.

Velocity of the rack cutter

$$\boldsymbol{V}_{\mathrm{h}}^{(\mathrm{F})} = -r_1\omega_1\boldsymbol{j}_{\mathrm{h}} \tag{41}$$

Velocity of the contact point of the helical cutting tool

$$\begin{aligned}\boldsymbol{V}_{\mathrm{h}}^{1} &= \boldsymbol{\omega}_1 \times \boldsymbol{r}_1'' \\ &= \overline{\boldsymbol{O}_{\mathrm{w}}\boldsymbol{O}_{\mathrm{h}}} \times \boldsymbol{\omega}_1 + \boldsymbol{\omega}_1 \times \boldsymbol{r}_{\mathrm{w}}\end{aligned} \tag{42}$$

where

$$\overline{\boldsymbol{O}_{\mathrm{w}}\boldsymbol{O}_{\mathrm{h}}} = (-r_1 + c)\boldsymbol{i}_{\mathrm{h}} + r_1\phi_1\boldsymbol{j}_{\mathrm{h}} \tag{43}$$

The relative velocity can be obtained as

$$\boldsymbol{V}_{\mathrm{h}}^{(\mathrm{F1})} = \boldsymbol{V}_{\mathrm{h}}^{(\mathrm{F})} - \boldsymbol{V}_{\mathrm{h}}^{(1)} \tag{44}$$

5.1 Profile generated by the left cutting face

The relative velocity of the contact point between region I and the generated helical cutting tool is

$$\begin{aligned}\boldsymbol{V}_{\mathrm{h}}^{(\mathrm{F1})} = -\omega_1\Bigg[\Bigg(b_0 - \frac{R}{\tan(45 + \psi_{\mathrm{L}}/2)} - \mathrm{HKW}\tan\psi_{\mathrm{L}} \\ + R\cos\psi_{\mathrm{L}} + \ell^{(\mathrm{I})}\sin\psi_{\mathrm{L}}\Bigg)\sin\lambda \pm u\cos\lambda - r_1\phi_1\Bigg] \\ \times \boldsymbol{i}_{\mathrm{h}} + \omega_1(R - \mathrm{HKW} - R\sin\psi_{\mathrm{L}} \\ + \ell^{(\mathrm{I})}\cos\psi_{\mathrm{L}} - c)\boldsymbol{j}_{\mathrm{h}}\end{aligned} \tag{45}$$

Substituting the unit normal vector shown in equation (23) and the relative velocity shown in equation (45) into $\boldsymbol{n} \cdot \boldsymbol{V}_{\mathrm{h}}^{(\mathrm{FI})} = 0$, the equation of meshing becomes

$$\begin{aligned}u = \mp(R - \mathrm{HKW} + \ell^{(\mathrm{I})}\cos\psi_{\mathrm{L}} - c)\tan\lambda\cot\psi_{\mathrm{L}} \\ \mp\Bigg(b_0 - \frac{R}{\tan(45 + \psi_{\mathrm{L}}/2)} - \mathrm{HKW}\tan\psi_{\mathrm{L}} \\ + \ell^{(\mathrm{I})}\sin\psi_{\mathrm{L}}\Bigg)\tan\lambda \pm \frac{r_1\phi_1}{\cos\lambda}\end{aligned} \tag{46}$$

Solving equation (46) and the locus equation (equation (35)) simultaneously, the generated tooth profile by region I can thus be obtained.

5.2 Profile generated by the right cutting face

The relative velocity of the contact point between region II and the generated helical cutting tool is

$$\begin{aligned}\boldsymbol{V}_{\mathrm{h}}^{(\mathrm{F1})} = -\omega_1\Bigg[\Bigg(-b_0 + \frac{R}{\tan(45+\psi_{\mathrm{R}}/2)} + \mathrm{HKW}\tan\psi_{\mathrm{R}} \\ -R\cos\psi_{\mathrm{R}} - \ell^{(\mathrm{II})}\sin\psi_{\mathrm{R}}\Big)\sin\lambda \pm u\cos\lambda - r_1\phi_1\Bigg] \\ \times \boldsymbol{i}_{\mathrm{h}} + \omega_1(R - \mathrm{HKW} - R\sin\psi_{\mathrm{R}} \\ + \ell^{(\mathrm{II})}\cos\psi_{\mathrm{R}} - c)\boldsymbol{j}_{\mathrm{h}} \end{aligned} \tag{47}$$

Substituting the unit normal vector shown in equation (25) and the relative velocity shown in equation (47) into $\boldsymbol{n}\cdot\boldsymbol{V}_{\mathrm{h}}^{(\mathrm{Fl})} = 0$, the equation of meshing becomes

$$\begin{aligned} u = \pm(R - \mathrm{HKW} + \ell^{(\mathrm{II})}\cos\psi_{\mathrm{R}} - c)\tan\lambda\cot\psi_{\mathrm{R}} \\ \pm\left(b_0 - \frac{R}{\tan(45+\psi_R/2)} - \mathrm{HKW}\tan\psi_{\mathrm{R}} \right. \\ \left. + \ell^{(\mathrm{II})}\sin\psi_{\mathrm{R}}\right)\tan\lambda \pm \frac{r_1\phi_1}{\cos\lambda} \end{aligned} \tag{48}$$

Solving equations (48) and (36) simultaneously, the generated tooth profile by region II can thus be obtained.

5.3 Profile generated by the fillet cutting face (region III)

The relative velocity of the contact point between region III and the generated helical cutting tool is

$$\begin{aligned}\boldsymbol{V}_{\mathrm{h}}^{(\mathrm{F1})} = -\omega_1\Bigg[\Bigg(b_0 - \frac{R}{\tan(45+\psi_{\mathrm{L}}/2)} - \mathrm{HKW}\tan\psi_{\mathrm{L}} \\ + R\sin\theta_{\mathrm{I}}\Big)\sin\lambda \pm u\cos\lambda - r_1\phi_1\Bigg]\boldsymbol{i}_{\mathrm{h}} \\ + \omega_1(R - \mathrm{HKW} - R\cos\theta_{\mathrm{I}} - c)\boldsymbol{j}_{\mathrm{h}} \end{aligned} \tag{49}$$

Substituting the unit normal vector shown in equation (27) and the relative velocity shown in equation (49) into $\boldsymbol{n}\cdot\boldsymbol{V}_{\mathrm{h}}^{(\mathrm{Fl})} = 0$, the equation of meshing becomes

$$\begin{aligned}\phi_1 = \Bigg\{\Bigg[b_0 - \frac{R}{\tan(45+\psi_{\mathrm{L}}/2)} - \mathrm{HKW}\tan\psi_{\mathrm{L}}\Bigg]\sin\lambda \\ \pm u\cos\lambda + (R - \mathrm{HKW} - c)\tan\theta_{\mathrm{I}}\sin\lambda\Bigg\}\Big/ r_1 \end{aligned} \tag{50}$$

Solving equations (50) and (37) simultaneously, the generated tooth profile by region III can thus be obtained.

5.4 Profile generated by the fillet cutting face (region IV)

The relative velocity of the contact point between region IV and the generated helical cutting tool is

$$\begin{aligned}\boldsymbol{V}_{\mathrm{h}}^{(\mathrm{F1})} = -\omega_1\Bigg[\Bigg(-b_0 + \frac{R}{\tan(45+\psi_{\mathrm{R}}/2)} + \mathrm{HKW}\tan\psi_{\mathrm{R}} \\ - R\sin\theta_{\mathrm{II}}\Big)\sin\lambda \pm u\cos\lambda - r_1\phi_1\Bigg]\boldsymbol{i}_{\mathrm{h}} \\ + \omega_1(R - \mathrm{HKW} - R\cos\theta_{\mathrm{II}} - c)\boldsymbol{j}_{\mathrm{h}} \end{aligned} \tag{51}$$

Substituting the unit normal vector shown in equation (29) and the relative velocity shown in equation (51) into $\boldsymbol{n}\cdot\boldsymbol{V}_{\mathrm{h}}^{(\mathrm{Fl})} = 0$, the equation of meshing becomes

$$\begin{aligned}\phi_1 = \Bigg[\Bigg(-b_0 + \frac{R}{\tan(45+\psi_{\mathrm{R}}/2)} + \mathrm{HKW}\tan\psi_{\mathrm{R}}\Big)\sin\lambda \\ \pm u\cos\lambda - (R - \mathrm{HKW} - c)\tan\theta_{\mathrm{II}}\sin\lambda\Bigg]\Big/ r_1 \end{aligned} \tag{52}$$

Solving equations (52) and (48) simultaneously, the generated tooth profile by region IV can thus be obtained.

5.5 Profile generated by the top land cutting face

The relative velocity of the contact point between the top land cutting face and the generated helical cutting tool is

$$\begin{aligned}\boldsymbol{V}_{\mathrm{h}}^{(\mathrm{F1})} = -\omega_1\Bigg[\Bigg(-b_0 + \frac{R}{\tan(45+\psi_{\mathrm{R}}/2)} \\ + \mathrm{HKW}\tan\psi_{\mathrm{R}} + \mu\Big)\sin\lambda \pm u\cos\lambda - r_1\phi_1\Bigg]\boldsymbol{i}_{\mathrm{h}} \\ + \omega_1(-\mathrm{HKW} - c)\boldsymbol{j}_{\mathrm{h}} \end{aligned} \tag{53}$$

Substituting the unit normal vector shown in equation (31) and the relative velocity shown in equation (53) into $\boldsymbol{n}\cdot\boldsymbol{V}_{\mathrm{h}}^{(\mathrm{Fl})} = 0$, the equation of meshing becomes

$$\begin{aligned} u = \mp\Bigg[-b_0 + \frac{R}{\tan(45+\psi_{\mathrm{R}}/2)} \\ + \mathrm{HKW}\tan\psi_{\mathrm{R}} + \mu\Bigg]\tan\lambda \pm \frac{r_1\phi_1}{\cos\lambda} \end{aligned} \tag{54}$$

Solving equations (54) and (39) simultaneously, the generated tooth profile by the top land cutting face can thus be obtained.

Table 1 Parameters of rack cutter and helical cutting tool

Parameters of shifted helical cutting tool				Parameters of rack cutter	
Circular pith (CP)	2.8			Addendum (HKW)	1.48
Module (m)	0.89126			Dedendum (HFW)	0.29
Number of teeth, T	12			Tooth thickness of rack cutter ($2b_0$)	1.92
Height of chamfering, e	0.2			Radius of rack cutter, r	0.15
Whole depth (mm) (HKW + HFW)	1.77			Pressure angle of left cutting face, ψ_L	45°
Length of cutter (mm)	30			Pressure angle of right cutting face, ψ_R	3°
Pitch diameter (mm)	15.125			Pressure angle of chamfering, ψ_3	66°
Helix angle (deg)	45				
Shifted amount, c	+0.2	+0.0	−0.2		
Outside diameter, D	16.10	15.70	15.30		
Root diameter, d	12.57	12.17	11.77		

5.6 Profile generated by the chamfering cutting face

The relative velocity of the contact point between the chamfering cutting face and the generated helical cutting tool is

$$\begin{aligned} \boldsymbol{V}_h^{(F1)} = &-\omega_1\{[b_0 + (\mathrm{HFW} - e)\tan\psi_L + \ell^{(VI)}\sin\psi_3]\sin\lambda \\ &\pm u\cos\lambda - r_1\phi_1\}\boldsymbol{i}_h \\ &+ \omega_1(\mathrm{HFW} - e + \ell^{(VI)}\cos\psi_3 - c)\boldsymbol{j}_h \end{aligned} \tag{55}$$

Substituting the unit normal vector shown in equation (33) and the relative velocity shown in equation (55) into $\boldsymbol{n}\cdot\boldsymbol{V}_h^{(FI)} = 0$, the equation of meshing becomes

$$\begin{aligned} u = &\mp(\mathrm{HFW} - e + \ell^{(VI)}\cos\psi_3 - c)\tan\lambda\cot\psi_3 \mp [b_0 \\ &+ (\mathrm{HFW} - e)\tan\psi_L + \ell^{(VI)}\sin\psi_3] \\ &\times\tan\lambda + \frac{r_1\phi_1}{\cos\lambda} \end{aligned} \tag{56}$$

Solving equations (56) and (40) simultaneously, the generated tooth profile by the chamfering cutting face can thus be obtained.

Example 1

The characteristics of a helical cutting tool are shown in Table 1. The solid model of the helical cutting tool can be generated by the proposed mathematical model and the parameter of the shifted helical cutting tool. In this paper, the designed profile of the rack cutter is shown in Fig. 5, and Fig. 6 shows the tooth profile and the simulated motion paths of the helical cutting tool. Figure 7 shows the transverse section of the helical cutting tool with different shifted distances. When the outside diameter is constant, the transverse sections of the helical cutting tool with the different shifted distances are shown in Fig. 8. Figures 9 and 10 are respectively the right- and left-hand helix solid models of the helical cutting tool with shifted distance $c = 0$.

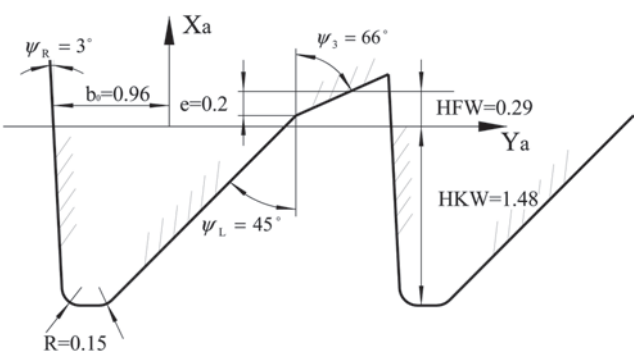

Fig. 5 Profile of the novel designed rack cutter

6 CHARACTERISTICS OF THE HELICAL CUTTING TOOL

The characteristics of the helical cutting tool have important effects on cutting quality and efficiency. In this section, by applying the mathematical model of the helical cutting tool proposed in the previous section and the characteristics of involute gear, the condition of full undercutting, cutting angles, and the width of the top land of the helical cutting tool are derived.

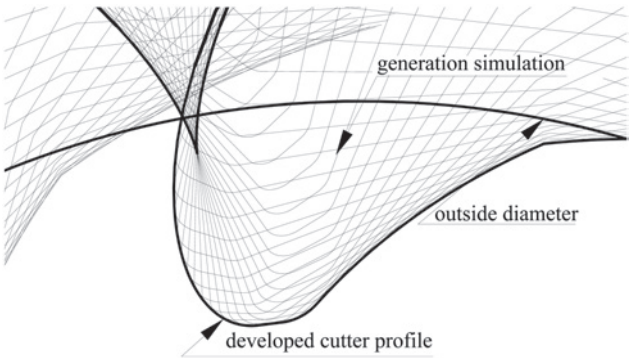

Fig. 6 Tooth profile and generation simulation of the helical cutting tool

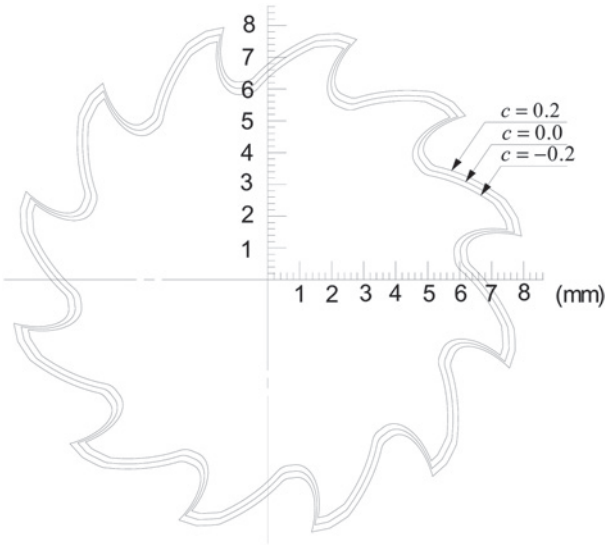

Fig. 7 Generated tooth profile with different shifted distances

Fig. 9 Solid modelling of the right-hand helical cutting tool

6.1 Full undercutting condition

As mentioned, the phenomenon of undercutting on gears is utilized to generate the right cutting face of the helical cutting tool by the fillet cutting face of the rack cutter. Figure 11 shows a poorly designed rack cutter, where only part of an involute curve is generated on the cutting tool. In view of the importance of undercutting on forming helical tool cutting tools, this phenomenon is studied mathematically here. In Fig. 11, when the cutting edge undercuts fully, the intersection point, P, between the right cutting face and the undercutting portion is located beyond the outer diameter of helical cutting tool. Thus, the right cutting face yields equations (36) and (48), while equations of the undercutting portion are given in equations (38) and (52). When $r_P > r$, full undercutting of the helical cutting tool occurs.

Example 2

The characteristics of a helical cutting tool are shown in Table 1, where the shifted distance, c, is zero. For this tool, the radius of the intersection point

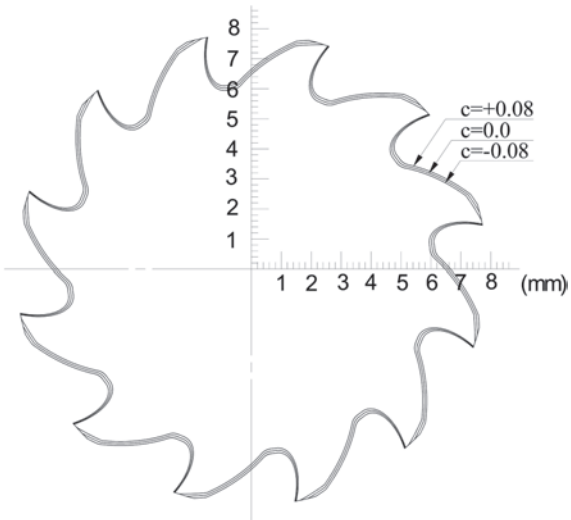

Fig. 8 Generated tooth profile with different shifted distances (outside diameter is constant)

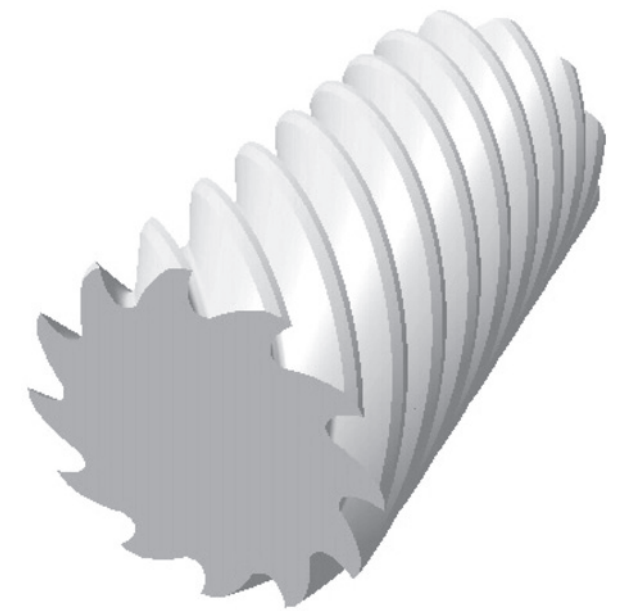

Fig. 10 Solid modelling of the left-hand helical cutting tool

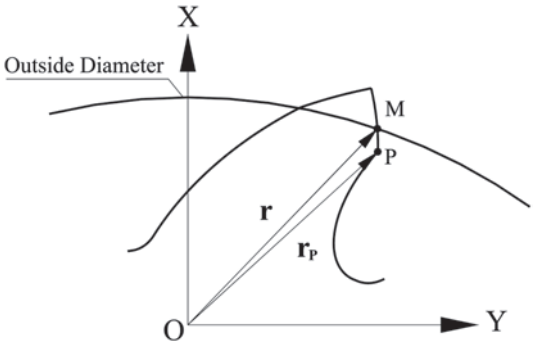

Fig. 11 Non-full undercutting of the helical cutting tool

P ($r_P = 7.874$) is larger than the outer radius of the cutting tool ($r = 7.853$), and therefore the design of the rack cutter has satisfied the requirement of full undercutting on the helical cutting tool.

6.2 Definition of the cutting angles of the helical cutting tool

The cutting angles at the end section profile are defined in Fig. 12. Point A is the intersection point of the undercut portion (region IV) and the circumference of the helical cutting tool. Point B is the intersection point of the chamfered edge and the circumference of the helical cutting tool, and point E is the intersection point of the left cutting edge and the chamfered cutting edge. Vectors $\boldsymbol{T}'_{\mathrm{A}}$ and $\boldsymbol{T}_{\mathrm{A}}$ are the tangential and positional vectors of point A respectively. Vector $\boldsymbol{T}_{\mathrm{B}}$ is the tangential vector of point B, $\boldsymbol{T}'_{\mathrm{B}}$ is the tangential vector of the chamfered cutting edge at point B, and $\boldsymbol{T}_{\mathrm{E}}$ is the tangential vector of the chamfered cutting edge at point E. The radial rake angle γ_{A} is the angle between $\boldsymbol{T}_{\mathrm{A}}$ and $\boldsymbol{T}'_{\mathrm{A}}$, the relief angle γ_{B} is the angle between $\boldsymbol{T}_{\mathrm{B}}$ and $\boldsymbol{T}'_{\mathrm{B}}$, and the clearance angle γ_{E} is the angle between $\boldsymbol{T}_{\mathrm{B}}$ and $\boldsymbol{T}_{\mathrm{E}}$.

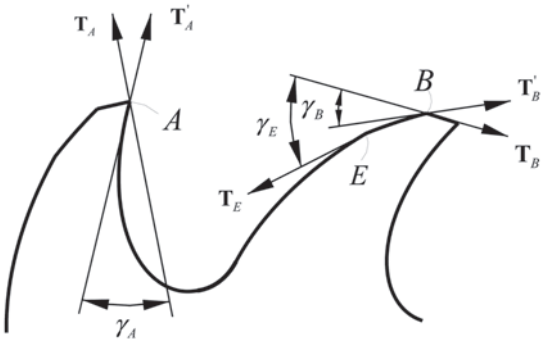

Fig. 12 Definitions of the cutting angles

6.2.1 *Analysis of the radial rake angle* γ_{A}

In Fig. 12, the outer diameter of the helical cutting tool is $2(r_1 + \mathrm{HFW})$, where r_1 is the radius of the pitch circle of the helical cutting tool and HFW is the addendum of the helical cutting tool. If (x_A, y_A) are the coordinates of point A, then

$$\sqrt{x_{\mathrm{A}}^2 + y_{\mathrm{A}}^2} = r_1 + \mathrm{HFW} \tag{57}$$

By substituting the equations of point A shown in equations (38) and (52) into the above equation, ϕ_1, and therefore $\boldsymbol{T}_{\mathrm{A}}$ and $\boldsymbol{T}'_{\mathrm{A}}$, can be obtained. Angle γ_{A} is then calculated by the vector dot product of $\boldsymbol{T}_{\mathrm{A}}$ and $\boldsymbol{T}'_{\mathrm{A}}$.

6.2.2 *Analysis of the relief angle* γ_{B}

As the involute curve is an extension of the base circle, the normal vector of the involute curve at point B is tangent to the base circle shown in Fig. 13. Vector ***OG*** is thus in the same direction as $\boldsymbol{T}'_{\mathrm{B}}$ at point B. The relationship between the involute pressure angle and the radius of the base circle, r_{b}, can be shown as

$$r_{\mathrm{B}} \cos \psi_{\mathrm{B}} = r_{\mathrm{b}} \tag{58}$$

where r_{B} is the radius of point B.

As vectors $\boldsymbol{T}_{\mathrm{B}}$ and $\boldsymbol{T}'_{\mathrm{B}}$ are perpendicular to ***BO*** and ***BG*** respectively, the relief angle γ_{B} is obtained as

$$\gamma_{\mathrm{B}} = \frac{\pi}{2} - \psi_{\mathrm{B}} \tag{59}$$

6.2.3 *Analysis of the clearance angle* γ_{E}

In Fig. 14, $\boldsymbol{T}_{\mathrm{E}}$ is the tangential vector at point E while $\boldsymbol{T}'_{\mathrm{E}}$ is the vector perpendicular to the position

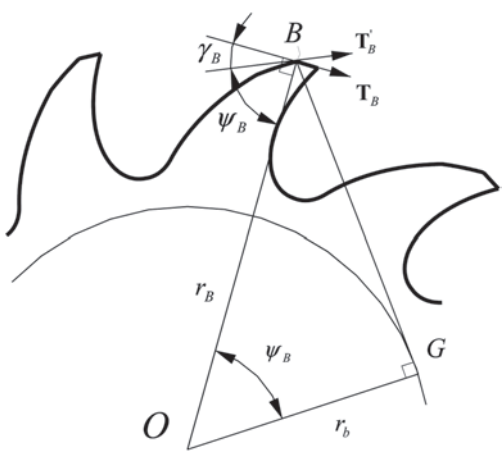

Fig. 13 Relief angle at point B

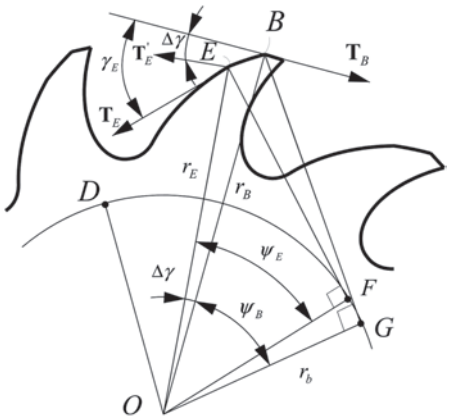

Fig. 14 Relationship between clearance angle γ_E and Δ_γ at point E

vector $\boldsymbol{r}_E$. Applying the theory of involute, the clearance angle γ_E is obtained as

$$\gamma_E = \frac{\pi}{2} + \Delta\gamma - \psi_E \tag{60}$$

where

$$\Delta\gamma = \text{inv}\psi_B - \text{inv}\psi_E \tag{61}$$

6.3 Effect of shifted distance on cutting angles

Shifted distances in the hobbing process have significant effects on generating the cutting angles of the helical cutting tool. By substituting the properties of the helical cutting tool shown in Table 1 into the above-derived equations, the corresponding cutting angles can be determined for different shifted distance values. Figure 15 presents the variation in cutting angles when the outer diameters are changed

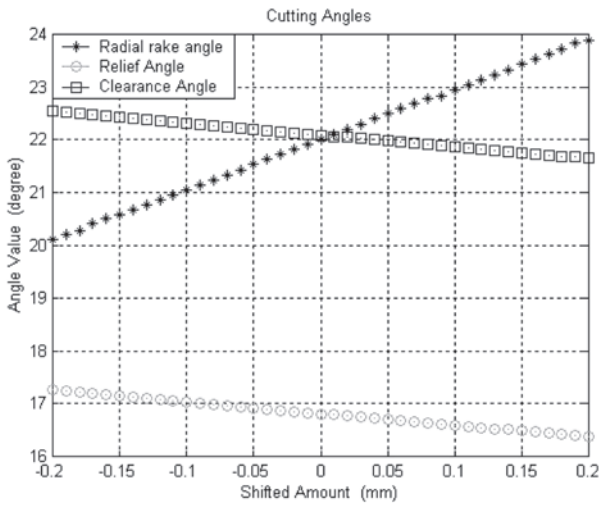

Fig. 15 Variation in cutting angles when the outside diameters are changed according to the shifted distance

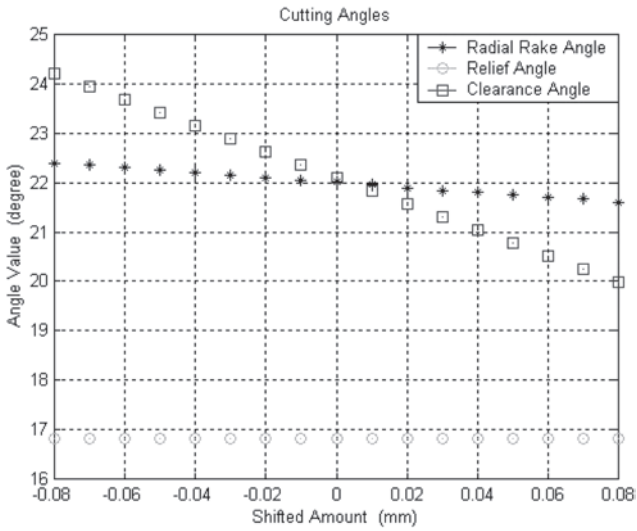

Fig. 16 Cutting angles when the outside diameters are constant

according to the shifted distance. For comparison, Fig. 16 shows the variation in cutting angles with a constant outer diameter.

6.4 Width of the top land of the helical cutting tool

The width of the top land of a helical cutting tool greatly influences the life of a cutting tool. In helical cutting tools, the left cutting face and the chamfering cutting face are involute curves, which thus allow the use of involutometry to determine the width of the top land of the helical cutting tool. The pressure angles at different points are shown in Fig. 17. Figure 18 shows the relationship between the tooth thickness and the pitch line of the rack cutter.

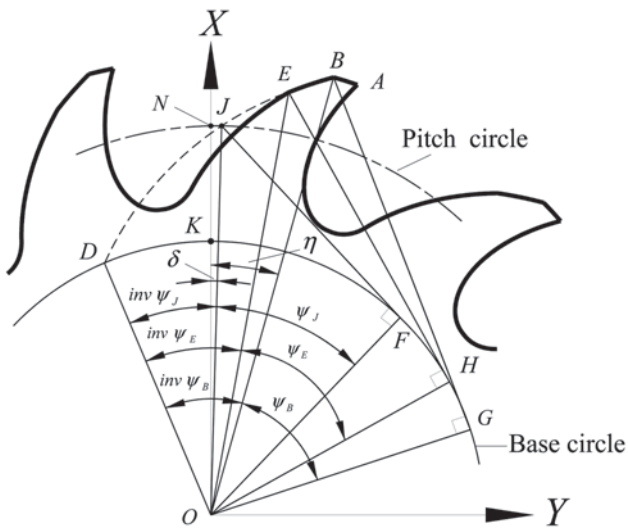

Fig. 17 Pressure angles at different points

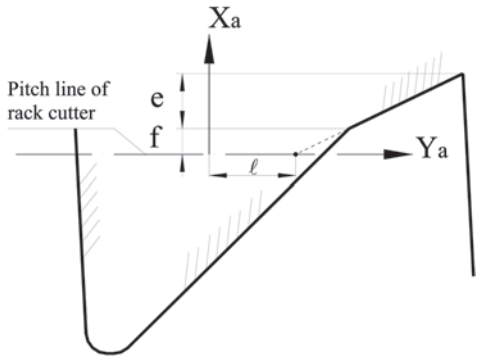

Fig. 18 Tooth thickness relationship on the pitch line

From geometry analysis shown in Fig. 17, η can be expressed as

$$\eta = \angle\mathrm{KOJ} + \angle\mathrm{JOB} \tag{62}$$

where

$$\angle\mathrm{JOB} = \mathrm{inv}\psi_\mathrm{B} - \mathrm{inv}\psi_\mathrm{J} \tag{63}$$

In Fig. 17, point D is the start point of the involute curve while point J is the intersection point between this curve and the pitch circle. At point J, ψ_J is the pressure angle and $\mathrm{inv}\psi_\mathrm{J}$ is the corresponding involute function. Assuming pure rolling between the pitch line of the rack cutter and the pitch circles of the generated gears, the arc length, NJ, shown in Fig. 17 is equal to the distance ℓ shown in Fig. 18. The angle $\delta = \angle\mathrm{KOJ}$ is therefore

$$\delta = \frac{\ell}{r_1} \tag{64}$$

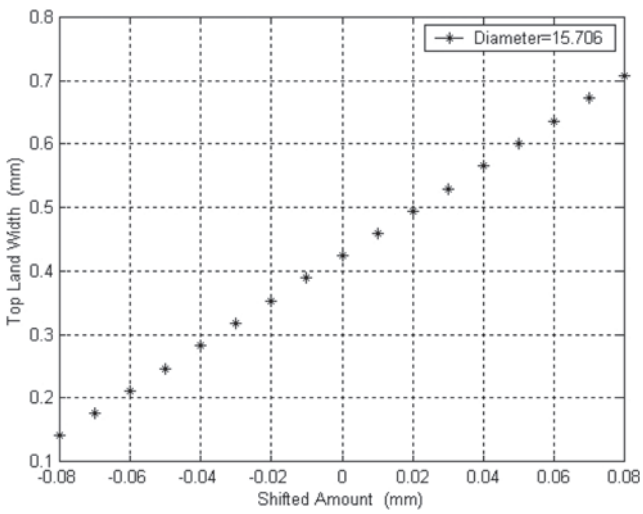

Fig. 19 Width of the top land of the helical cutting tool with a constant outside diameter

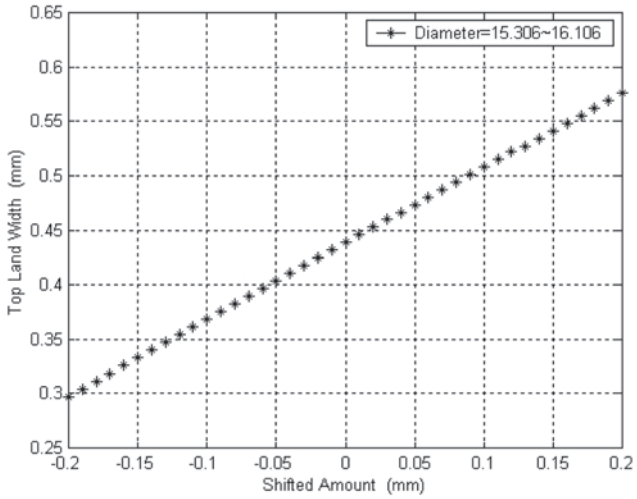

Fig. 20 Width of the top land of the helical cutting tool with a variable outside diameter according to the shifted distance

giving

$$\eta = \mathrm{inv}\psi_\mathrm{B} - \mathrm{inv}\psi_\mathrm{J} + \delta \tag{65}$$

For the helical cutting tool shown in Table 1, Figs 19 and 20 show the width of the calculated top land of the helical cutting tool for constant outer diameters and for outer diameters changing according to the shifted distance respectively.

7 CONCLUSION

In this paper, a novel cutter for manufacturing a multiangle helical cutting tool in one hobbing process has been designed. The cutting profile of the cutter was designed as three straight edges having different pressure angles and two arcs. Mathematical models of the generated helical cutting tool profile have been derived and used to determine the cutting angles, the full undercutting condition, and the width of the top land. A computer simulation has also been carried out to validate the mathematical model. This established technique can be used as design guidance for future new cutters, in particular for cutters that generate a multiangle helical cutting tool. Therefore, it is anticipated that results from this paper will contribute to the improvement in the manufacture of helical cutting tools and provide the tool industry with a design reference for machining similar tools. The results can also serve a basis for researchers to optimize and improve their tool designs.

ACKNOWLEDGEMENT

The work outlined in this paper was supported by the National Science Council of the Republic of China under grants NSC91-2212-E-150-022 and NSC92-2212-E-150-031.

REFERENCES

1 **Koelsch, J. R.** Hobs in high gear. *Mfg Engng*, 1994, 67–69.
2 **Phillips, R.** New innovations in hobbing. Part I. *Gear Technol.*, 1994, 16–20.
3 **Bouzakis, K. D.** and **Antonidais, A.** Optimizing of tangential tool shift in gear hobbing. *Ann. CIRP*, 1995, **44**(1), 75–78.
4 **Ainoura, M.** and **Nagano, K.** The effect of reverse hobbing at a high speed. *Gear Technol.*, 1987, 8–15.
5 **Cluff, B. W.** Effects of hob quality and resharpening errors on generating accuracy. *Gear Technol.*, 1987, 37–46.
6 **Tsay, C. B.** Helical gears with involute shaped teeth: geometry, computer simulation, tooth contact analysis, and stress analysis. *Trans. ASME, J. Mechanisms, Transm., and Automn in Des.*, 1988, **110**, 482–491.
7 **Chang, S. L., Tsay, C. B.,** and **Nagata, S.** A general mathematical model for gear generated by CNC hobbing machine. *Trans. ASME, J. Mech. Des.*, 1997, **119**, 108–113.
8 **Chang, S. L., Tsay, C. B.,** and **Tseng, C. H.** Kinematic optimization of a modified helical simple gear train. *Trans. ASME, J. Mech. Des.*, 1997, **119**, 307–314.
9 **Chang, S. L., Tsay, C. B.,** and **Wu, L. I.** Mathematical model and undercutting analysis of elliptical gear generated by rack cutters. *Mechanism and Mach. Theory*, 1996, **31**(7), 879–890.
10 **Chang, S. L.** Gear hobbing simulation of CNC gear hobbing machines. Doctoral dissertation, National Chaio Tung University, Hsinchu, Taiwan.
11 **Kapelevich, A.** Geometry and design of involute spur gears with asymmetric teeth. *Mechanism and Mach. Theory*, 2000, **35**, 117–130.
12 **Liu, J. Y.** and **Chang, S. L.** Design of hob cutters for generating helical cutting tools with multi-cutting angles. *Int. J. Mach. Tools and Mf.*, 2003, **43**, 1185–1195.

APPENDIX

Notation

$2b_0$	tooth thickness of the rack cutter
c	shifted amount between the helical cutting tool and the rack cutter
D	outside diameter of the helical cutting tool
e	height of chamfering from point q to the root of a tooth of the rack cutter
HKW, HFW	addendum and dedendum of the rack cutter
$\text{inv}\psi_i$	involute function of ψ_i
$\ell^{(\text{I})}, \ell^{(\text{II})}, \ell^{(\text{VI})}$	parameters of vectors $\boldsymbol{r}_{\text{a}}^{(\text{I})}, \boldsymbol{r}_{\text{a}}^{(\text{II})}$, and $\boldsymbol{r}_{\text{a}}^{(\text{VI})}$ respectively
$[\boldsymbol{M}_{ij}]$	transformation matrix from system S_j to system S_i
$\boldsymbol{n}_i^k$	unit normal vector of the contact point on the kth portion in coordinate system S_i
$\boldsymbol{N}_i^k$	normal vector of the contact point on the kth portion in coordinate system S_i
O_i	origin of coordinate system S_i
P_0	circular pitch of the rack cutter
r	outside radius of the helical cutting tool
r_b	radius of the base circle of involute BE
r_{B}	radius of point B
r_1	radius of the pitch circle of the helical cutting tool
$\boldsymbol{r}_i^{(n)}$	vectors of cutting edge n in coordinate system S_i
$\boldsymbol{r}_1'$	position vector of the contact point in the coordinate system S_1
R	radius of the rack cutter fillet
S_{a}	coordinate system of the rack cutter
S_h	fixed coordinate system
S_{w}	coordinate system of the helical rack cutter
S_1	coordinate system of the helical cutter tool
$\boldsymbol{T}_{\text{A}}', \boldsymbol{T}_{\text{A}}$	tangential and positional vectors of point A
$\boldsymbol{T}_{\text{B}}$	tangential vector of point B
$\boldsymbol{T}_{\text{B}}'$	tangential vector of the chamfered cutting edge at point B
$\boldsymbol{T}_{\text{E}}$	tangential vector of the chamfered cutting edge at point E
u	distance between origins O_{w} and O_{a}
$\boldsymbol{V}_{\text{h}}^{(\text{F})}$	velocity of the rack cutter in coordinate system S_{h}
$\boldsymbol{V}_{\text{h}}^{(\text{F1})}$	relative velocity of the contact point between regions I, II, III, IV, V, and VI and the generated helical cutting tool in coordinate system S_i
$\boldsymbol{V}_{\text{h}}^{(1)}$	velocity of the contact point of the helical cutting tool in coordinate system S_{h}

$\gamma_A, \gamma_B, \gamma_E$	radial rake angle, relief angle, and clearance angle of the helical cutting tool
δ	angle between points K and J
$\Delta\gamma$	angle between points B and E
η	angle between point B and J (point J is the intersection point between the involute curve and the pitch circle)
$\theta_I, \theta_{II}, \mu$	parameters of vectors $\boldsymbol{r}_a^{(III)}, \boldsymbol{r}_a^{(IV)}$, and $\boldsymbol{r}_a^{(V)}$
λ	lead angle of the helical cutting tool
ξ	pitch line of the rack cutter
ϕ_1	angular displacement of the helical cutting tool while hobbing
ψ_B, ψ_E, ψ_J	involute pressure angle of points B, E, J respectively
ψ_L, ψ_R, ψ_3	pressure angle of cutting edges I, II, and VI respectively
ω_1	angular velocity of the helical cutting tool while hobbing